

Observational Test for the Solar Wind Sputtering Origin of the Moon's Extended Sodium Atmosphere

Michael Mendillo, Jeffrey Baumgardner, and Jody Wilson

Center for Space Physics, Boston University, Boston, Massachusetts 02215

E-mail: mendillo@bu.edu

Received June 2, 1998; revised September 9, 1998

We present observations of the lunar sodium atmosphere during four lunar eclipses between 1993 and 1997. With the Moon inside the magnetosphere, and therefore shielded from solar wind impact, we find its Na atmosphere to be comparable in abundance to cases near first and third quarter, implying that solar wind ion sputtering is not a significant source of the atmosphere. The atmosphere is azimuthally symmetric, and it extends beyond the field of view of our observations (~12 Lunar radii). The average sodium atmospheric profile is best characterized by an $r^{-1.4}$ radial power law, close to that for an entirely escaping atmosphere. The average extrapolated near-surface brightness of 1145 rayleighs is in agreement with the near-surface polar brightness seen at quarter Moon. This corresponds to a line-of-sight neutral column content of 1.4×10^9 Na atoms cm^{-2} above the limb and a density of ~ 3 atoms cm^{-3} above the surface, decreasing as $r^{-2.4}$. We suggest that a blend of sources (15% micrometeor impact uniform over the surface and 85% photon-induced desorption dependent on solar-zenith angle over the sunlit hemisphere) could account for the observed extended sodium atmospheres.

© 1999 Academic Press

Key Words: Moon; atmospheres; evolution.

I. INTRODUCTION

The discovery of sodium and potassium gases above the lunar surface (Potter and Morgan 1988a, 1988b; Tyler *et al.* 1988) initiated a now decade-long series of observations and model studies of how the Moon's transient atmosphere is created and lost. Stern (1998) has provided an excellent summary of the current status of lunar atmospheric science and of how comparisons with Mercury, comets, asteroids, and the moons of the giant planets can lead to a better understanding of so-called "surface boundary exospheres" (SBEs) in the solar system. While similarities certainly exist among these bodies, it may well be the differences in their atmospheres that ultimately lead to comprehensive answers about their sources and sinks. For example, in each atmosphere in the solar system where Na and K have been detected, their ratio of abundance is unique to that body (Hunten and Sprague 1997). Similarly, the degree to which Na and K serve as tracers of more abundant elements, but ones not

so easily detected, surely varies at each site where they have been found. Yet the mechanisms of ejection from a regolith involve the same physical processes acting throughout the solar system. This duality of roles continues to dominate and to confuse the study of the lunar atmosphere: we study it as an important case in its own right and for its role as a conveniently nearby laboratory-in-space for detailed investigation of more remote SBEs in the solar system.

To date, no long-term monitoring effort for the Moon's atmosphere has been attempted, and thus the basis for progress has been a series of irregularly spaced observations. Given the relatively low number of published lunar atmosphere data sets, a remarkably high science yield has been achieved. Yet, for progress to continue, a new era of lunar observations, one that emphasizes temporal continuity and higher resolution, is required. For example, daily observations of the Moon's Na and K emissions for a full month, any month, would certainly be capable of addressing critically unanswered questions on variability of sources. For a single instrument to conduct such observations, a space-based platform is clearly required. Groundbased observations, certainly less costly but also dependent on local weather conditions, cannot realistically provide such a data base. What can be done, however, is more frequent observing campaigns aimed at a specific issue so that a particular mechanism can be addressed repeatedly in order to assess both its importance and its variability. In this paper we report on such a highly focused study, the impact of solar wind plasma as a sputtering source for the lunar atmosphere. Any sodium ions carried from the sun to the moon by the solar wind are considered completely negligible as a source of neutral sodium in comparison to the sodium liberated from the surface of the moon itself.

II. OBSERVATIONAL TESTS FOR MECHANISMS

Sodium atoms can be emitted from the Moon's regolith by a rich set of surface processes (e.g., Morgan and Shemansky 1991, Sprague *et al.* 1992, Smyth and Marconi 1995). Processes fall into four categories: *thermal desorption*, in which heating of the surface evaporates atoms and molecules off of the surface; *photon-stimulated desorption*, which involves an electronic

excitation of a target atom or molecule; *sputtering* by solar wind ions, which ejects atoms or molecules by either a cascade of momentum transfer collisions or chemical reactions which reduce the binding energies within the surface material; and meteorite *impact vaporization*. More detailed descriptions of sputtering and desorption processes are given by Johnson (1990), Potter (1995), and Madey *et al.* (1998). Madey *et al.* consider photon-stimulated desorption to be one form of a more general desorption process they call “desorption induced by electronic transitions.” They include in this category *electron-stimulated desorption*, a process which has not been addressed by the lunar atmosphere community.

The population of thermally desorbed Na atoms cannot have more energy than is available from the thermal conditions of the regolith ($T < 400^\circ\text{K}$), resulting in low thermal speeds ($V \leq .5 \text{ km/s}$) that do not allow Na to reach trajectory apex heights significantly above the surface, i.e., $\leq 100 \text{ km}$ or 0.06 lunar radii (R_M). Observationally, these low altitude atoms were the first ones detected. Later work showed that Na could be detected routinely to distances $>4-5 R_M$ (Mendillo *et al.* 1991, 1993; Flynn and Mendillo 1993), indicating that more energetic processes create the extended lunar atmosphere (Ip 1991, Flynn and Mendillo 1995, Smyth and Marconi 1995). The distinction between cold and hot populations (as discussed by Sprague *et al.* 1992 and Stern and Flynn 1995) is a separate issue from the *types* of superthermal sources responsible for the extended atmosphere itself, the topic of this study.

To formulate tests that might differentiate between the higher energy agents (sunlight, solar wind, micrometeors), there are obvious geometrical and temporal parameters to consider. These fall into four categories:

(a) Solar zenith angle tests: Photons and solar wind particles strike the regolith with a vertical energy flux that varies with solar zenith angle as $\cos(\chi)$. For a desorption yield that depended only on energy flux (as opposed, for example, to one with a more subtle dependence on angle of arrival into a lattice, or one dependent on mare vs highlands target composition), the resultant atmosphere would also depend on χ . For a spatially uniform source (as is often suggested for micrometeors), the resultant atmosphere would not have a strong χ -dependence (Ip 1991, Flynn and Mendillo 1995, Smyth and Marconi 1995). Observations by several groups using both spectroscopic and two-dimensional imaging techniques consistently reveal a χ -dependent sodium atmosphere at all altitudes sampled (Sprague *et al.* 1992, Flynn and Mendillo 1993, Mendillo *et al.* 1993, Cremonese and Verani 1997, Mendillo *et al.* 1997b, Potter and Morgan 1998). Thus, while a χ -dependent morphology can differentiate between uniform and solar-dependent sources, the specific role for each χ -dependent mechanism remains uncertain.

(b) Meteor shower tests: Observations during meteor showers, whether serendipitous (Hunten *et al.* 1991, Cremonese and Verani 1997, Sprague *et al.* 1998) or deliberate (Verani *et al.* 1998), bring a form of controlled, laboratory-in-space investigation to the issue of micrometeor sources. The upcoming Leonid

storm events of 1998 and 1999 should provide more definitive tests of this mechanism.

(c) Solar flare tests: For solar photon desorption, observations before and after a major solar flare formulate an experiment that, in practice, is difficult to carry out. Frequent observations during the upcoming solar cycle maximum years might allow for serendipitous results in this area.

(d) Solar wind tests: With *in-situ* monitoring of solar wind now possible, correlative studies of flow parameters, coronal mass ejection events, and lunar Na morphologies would be possible via more frequent observations from groundbased sites. A test which is more stringent, and observationally less dependent on chance occurrence of changes in the solar wind, is to monitor the lunar Na during the 3 to 4 days each month when the Moon passes through the tail portion of the Earth’s magnetosphere. This transition from the Moon being totally emersed in solar wind flow to one of total shielding is an ideal “active experiment” in space, as formulated by Potter and Morgan (1991, 1994). Unfortunately, monitoring these night-by-night Na brightness patterns requires about a week of telescope time with clear skies. Potter and Morgan did the next best thing, a statistical study of many non-consecutive data sets (45) from 1988–1993 that spanned quarter, gibbous, and full moon phases. These observations were made very close to the limb ($\sim 40 \text{ km}$ height) and showed a dramatic fall in brightness at the time of full Moon, i.e., when the Moon was in the center of the geomagnetic tail. The argument offered, quite reasonably, was that the solar wind impact effect must be a major source of sputtering Na from the regolith for most of the days of a month. However, as noted above, observations have demonstrated that the near-surface brightness in general depends on the local solar zenith angle; thus at the equator the near-surface brightness depends on viewing geometry (i.e., the phase of the moon). This can partly explain the results of Potter and Morgan.

III. ROLE OF LUNAR ECLIPSES

To determine the spatial extent of the lunar sodium atmosphere at the time of full Moon is a challenging observational problem. Given the importance of doing so as a test for the magnetospheric shielding issue, we devoted considerable attention to the problem. While our use of coronagraphic type masks to block the illuminated disk proved to be a successful technique at quarter Moon phase (Flynn and Mendillo 1993), bright scattered moonlight at times of gibbous and full Moon resulted in unreliable or null results (Mendillo *et al.* 1993). The opportunity to conduct an imaging experiment during the ~ 80 -min period of a total lunar eclipse occurred on 29 November 1993 with very favorable observing conditions at the McDonald Observatory. The results (Mendillo and Baumgardner 1995) were surprising in that the lack of scattered moonlight was so complete that it was possible to map lunar sodium at full Moon to distances greater than ever observed under quarter Moon conditions. Moreover, the radial decrease of an essentially azimuthally symmetrical coma matched the solar zenith angle pattern for $\chi = 90^\circ$ seen

above the poles of the Moon at quarter Moon phase. Such a robust atmosphere at the time when the Moon has been shielded from solar wind impact for days suggested that solar wind sputtering could not be a dominant source.

Our single eclipse night image of a prominent extended lunar atmosphere at full Moon was obviously in conflict with the several spectroscopic measurements used in the statistical study by Potter and Morgan (1994) to portray a negligible atmosphere much closer to the limb. While the dominant concern in any low-light-level imaging experiment (i.e., how to handle scattered light) is not an issue during a lunar eclipse, it was necessary to confirm independently the size and characteristics of the Moon's

sodium coma at full Moon. We now report on the results from three additional lunar eclipse campaigns, and on the comparison of these findings with those obtained on 29 November 1993.

IV. OBSERVATIONS

Figure 1 summarizes the four eclipse events used in this study, and Table I gives all of the observing mode parameters used during each event. The eclipses of 29 November 1993 and 27 September 1996 were observed using the 0.1-m telescope and bare CCD detector at the Boston University Station at the McDonald Observatory in Fort Davis, Texas. The event of 3–4

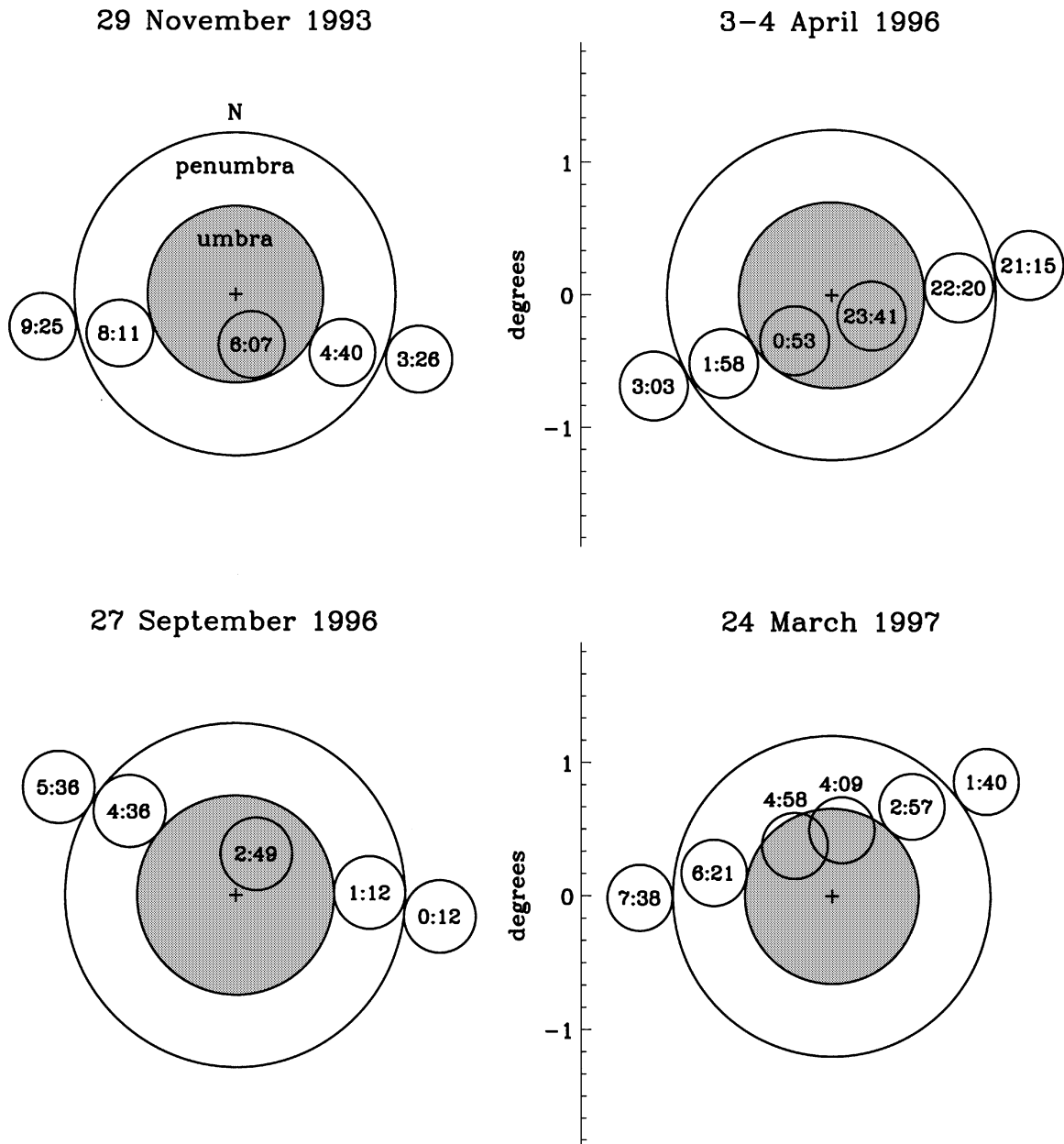


FIG. 1. The lunar eclipse events used in this study. All dates and times are in Universal Time (UT).

TABLE I
Observations

UT Date	UT Mid-eclipse	Site	Detector	Altitude (°)	Earth Na (R)
29/11/93	6:26	M	b	80	60 (u)
3-4/04/96	0:10	L	I	55	200 (u)
27/09/96	2:54	M	b	27	110 (o)
24/03/97	4:39	M	I	43	110 (o)

Note. M: McDonald Observatory; L: Las Palma; b: bare CCD; I: intensified CCD; u: from measurements in umbra; o: off-target measurements.

April 1996 was observed from the site of Italy’s new National Telescope Galileo (TNG) in La Palma (Canary Islands) using a portable telescope system and an image intensified CCD (Mendillo *et al.* 1997). The 24 March 1997 eclipse was recorded using the McDonald telescope with an image intensified CCD. In each case, the 0.1 m refractor was equipped with an occulting mask to ensure that even a faint glow from the eclipsed lunar disk would not enter the detector system. Baumgardner *et al.* (1993) give a full description of these imaging and detector systems.

The image processing method used for eclipse data has been described in Mendillo and Baumgardner (1995), and we include a brief discussion here. To insure uniformity of results, the November 1993 case was reanalyzed with the three new events. Off-band images at a wavelength of $6050 \text{ \AA} (\pm 7 \text{ \AA})$ are taken in conjunction with the on-band ($5893 \pm 6 \text{ \AA}$) images to measure scattered light from the Earth’s atmosphere and from the telescope optics. Both on-band and off-band images are bias-subtracted, dark-subtracted, and normalized to a flat field. The instrumental sensitivity to the solar spectrum reflected off the Moon is measured by imaging the Moon through a translucent white glass with each filter. We then subtract from the on-band images the corresponding off-band images weighted by the ratio of the on-band to off-band instrumental sensitivities. This effectively leaves only light from sodium atoms in the 5893 \AA images. The transmission of the Na ($D_1 + D_2$) lines through the sodium filter is measured by imaging light from a sodium vapor lamp through the filter and through an open filter position, and taking the ratio of the two images. This transmission factor is divided out of the 5893 \AA images. We calibrate the images in brightness units of rayleighs (R) by imaging a standard source through the sodium filter. The source is a disk coated with a phosphor containing carbon-14. The C_{14} decays and causes the phosphor to glow; independent calibrations of the standard source yield $81 \pm 10\% \text{ R/\AA}$ at 5893 \AA .

Some of the sodium emission in the data comes from the Earth’s atmosphere, and this must be subtracted from the images. During the September 1996 and March 1997 eclipses, we imaged the terrestrial sodium at large angular separations from the Moon. We subtract these brightness values from the lunar atmosphere images. For the November 1993 and April 1996 eclipses, we use the dimmest region of emission within the apparent location of the Earth’s umbra to estimate the average

terrestrial sodium brightness at the time the images were taken. In the latest two eclipses the darkest portion of the umbra was 10 to 30 R brighter than the terrestrial sodium measured off-target, so we assume a 20 R difference for the first two eclipses.

A special aspect of lunar eclipse image processing is the difficult (and sometimes controversial) method of determining brightness levels within the region spanned by the penumbra. Figure 2 shows processed images of the lunar atmosphere for two of the eclipses, with the locations of the umbra and penumbra indicated. Since the penumbral region is the portion of the image closest to the Moon, where brightness patterns can yield crucial radial behavior, particular care is given to the proper method of portraying these regions via a suitably chosen “penumbral light correction.” The goal is to capture the true sodium content that existed around the Moon on that night, that is, in the absence of the eclipse affecting the resonantly scattered sunlight that permits the detection of sodium. Figure 3 shows the four penumbral light correction curves used in the analyses. The curves are calculated numerically by measuring the total brightness of the unobstructed portion of the solar disk as seen from various locations around the Moon. Each was calculated separately for the Earth-Moon distance and Earth-Sun distance at the time of observation. A solar limb-darkening function

$$B(\theta)/B_0 = 1 - u - v + u \cdot \cos(\theta) + v \cdot \cos^2(\theta) \quad (1)$$

is assumed, where θ is 0° at the center of the sun’s disk and 90° at the limb, and $u = 0.88$ and $v = 0.23$ at 6000 \AA (Allen 1976). The images are divided by the penumbral function only down to the 50% illumination level in order to limit corrections to the observed brightness to factors of ≤ 2 . For the April 1996 and March 1997 eclipses, several images from each night are then coadded. In this way, the motion of the Moon through the Earth’s shadow allows a greater portion of the atmosphere to be sampled under more ideal illumination levels. The resulting images have an oval-shaped region around the Moon with no data; this region received less than 50% illumination throughout the observations. The fully processed and calibrated images of each eclipse event are presented in Fig. 4.

V. RESULTS

This unique set of images portrays a remarkable degree of consistency in the extended lunar atmosphere at the time of full Moon. The coma appears symmetrical, and it extends at least to the edge of the field of view. Due to the differences between the four eclipse geometries, the sizes of the occulting masks used, and the use of single bare CCD long exposure times versus multiple, coadded image-intensified short integrations, there is a nonuniformity in coverage of the regions close to the Moon. Figure 5 shows the radial profiles of the images sampled in azimuth at 30° clock angles. These illustrate a rather low degree of spatial variation in the radial patterns.

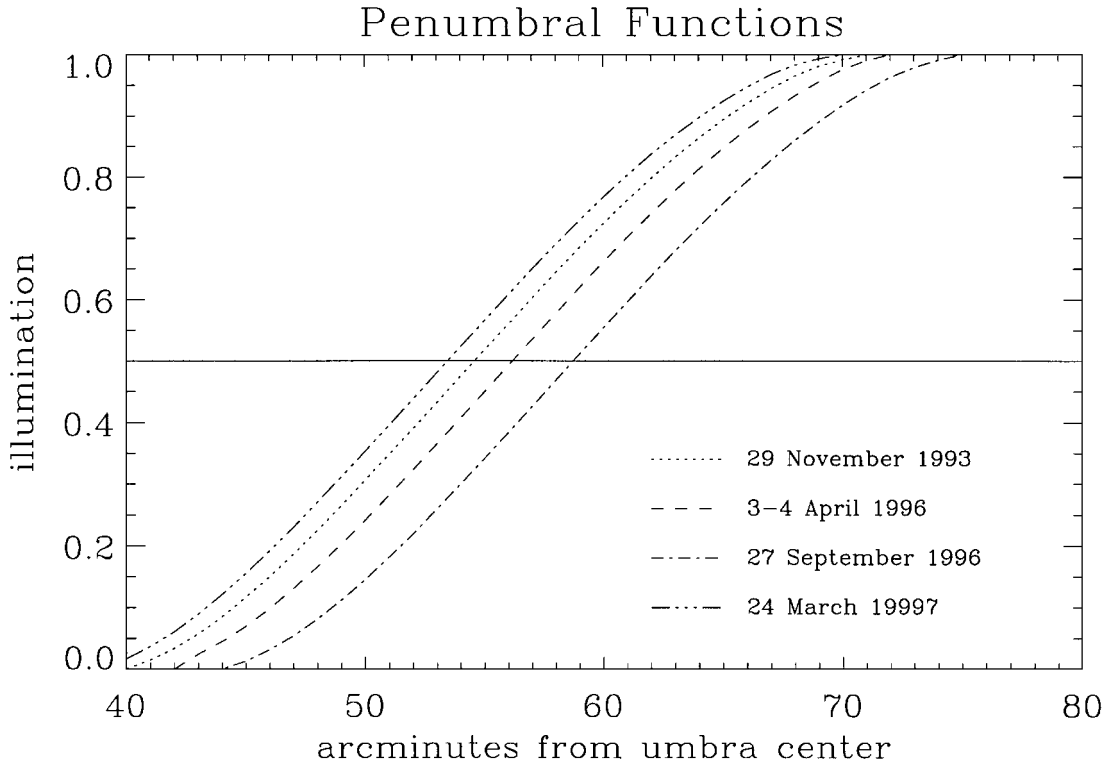


FIG. 3. The penumbral light correction functions used to convert observed brightness within the penumbral regions of reduced sunlight to effective total brightness from those regions in the absence of an eclipse (see text).

Consistent with our past analyses, we characterize each atmospheric profile with a radial power law of the form

$$I(r) = I_0 r^{-\alpha}, \quad (2)$$

where r is radial distance in units of lunar radii (R_M), I_0 is the extrapolated near-surface brightness, and α is the power law index. An $\alpha = 1$ corresponds to an escaping atmosphere, with larger values corresponding to a higher degree of it being bound. The least-squares fitted power laws are shown in Fig. 5. The power law parameters from fits at different position angles are plotted in Fig. 6, and show a high degree of azimuthal symmetry. The average image for all four eclipses is shown in Fig. 7, and the average radial profile is plotted in Fig. 8.

We next calculate the profile of number density in the lunar sodium atmosphere. For Na atoms traveling at ~ 1 km/s or less radially relative to the sun, the column abundance of sodium atoms along the line of sight is given by

$$N_{\text{los}}(r) = 1.2 \times 10^6 \cdot I(r) \quad (3)$$

(adapted from Brown and Young 1976), where I is the observed brightness (in rayleighs) at a distance r from the Moon ($r = 1$ at the limb). Higher heliocentric radial velocities result in more emission per sodium atom, so in the absence of direct velocity information, this is an upper limit to the line-of-sight column abundance. For simplicity, we assume that the atmosphere is spherically symmetric to obtain approximate number densities.

The number density can then be computed from the observed column abundance using the integral equation

$$n(r) = -(1/\pi) \int_r^\infty \frac{(dN_{\text{los}}(r_0)/dr_0) dr}{\sqrt{r_0^2 - r^2}} \quad (4)$$

(Roble and Hays 1972). When $N(r)$ is a power law, this equation has an analytic solution of the form

$$n(r) = 0.282 \cdot N_{\text{los}0} \alpha \cdot r^{-\alpha-1} \Gamma\left(\frac{\alpha+1}{2}\right) / \Gamma\left(\frac{\alpha+2}{2}\right), \quad (5)$$

where α is the power law index for the observed radial profile. Thus $n(r)$ is also a power law, with an index $(\alpha_n) = \alpha + 1$. The number density profile of an escaping atmosphere is a power law with $\alpha_n = 2$ (meaning $\alpha = 1$) because the area of an expanding “shell” of atmosphere is proportional to r^2 .

Our results compare favorably with previous work. The parameters for $n(r)$ for each eclipse are given in Table II. On average, the Na population we calculate from our observations has a near-surface density of 3 Na atoms cm^{-3} , near the lower limit of previous observations at high latitudes and/or solar zenith angles (5–14 cm^{-3} , Sprague *et al.* [1992]; 3.5–9.5 cm^{-3} , Cremonese and Verani [1997]; and 1.0–6.3 cm^{-3} , Sprague *et al.* [1998]). The near-surface number density for the April 1996 eclipse (2 cm^{-3}) agrees with the measurements taken on the same night

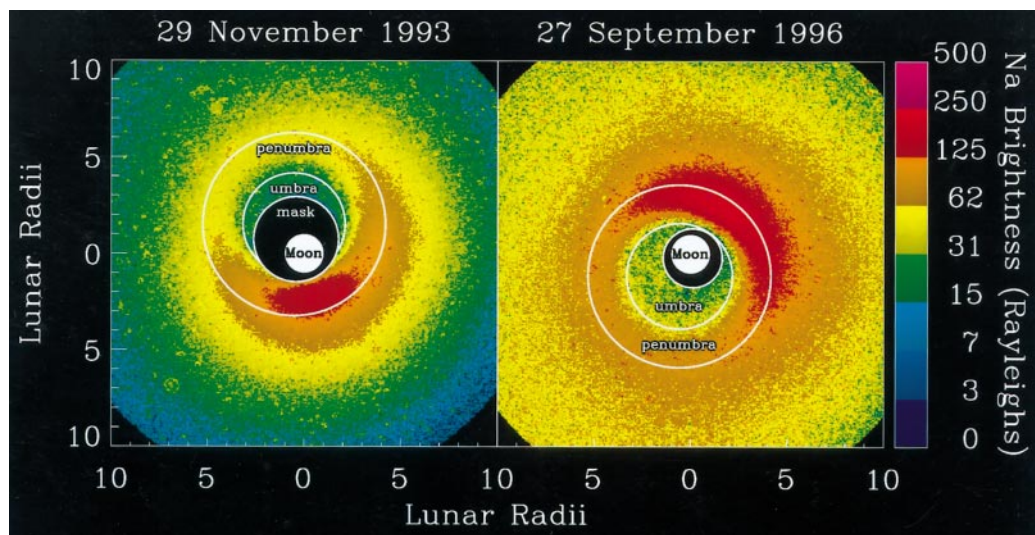


FIG. 2. Examples of processed images of two lunar Na atmospheres without the penumbral light correction.

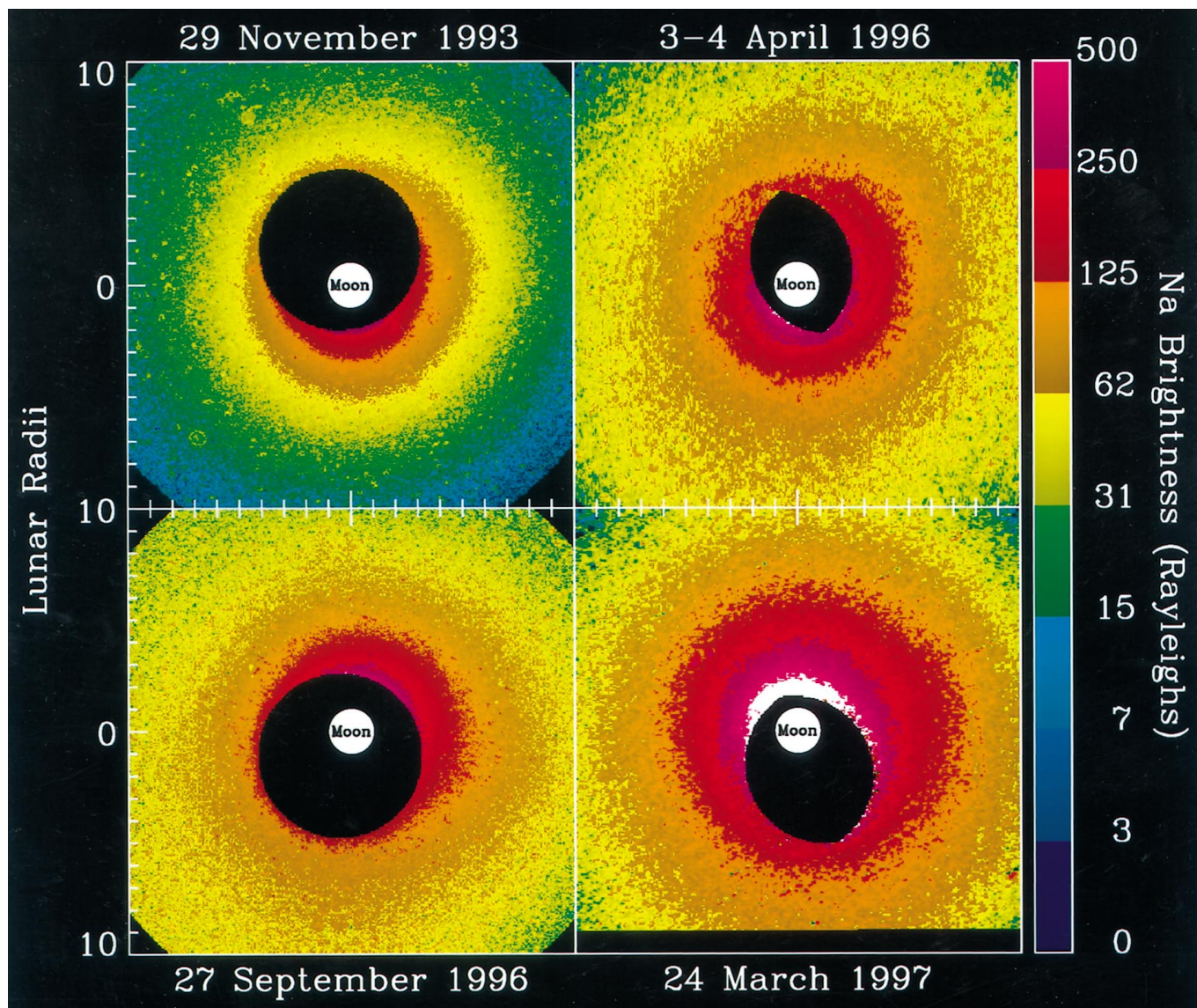


FIG. 4. The sodium atmosphere of the Moon as captured during four lunar eclipses. Brightness patterns in Rayleighs versus distance are presented in subsequent figures.

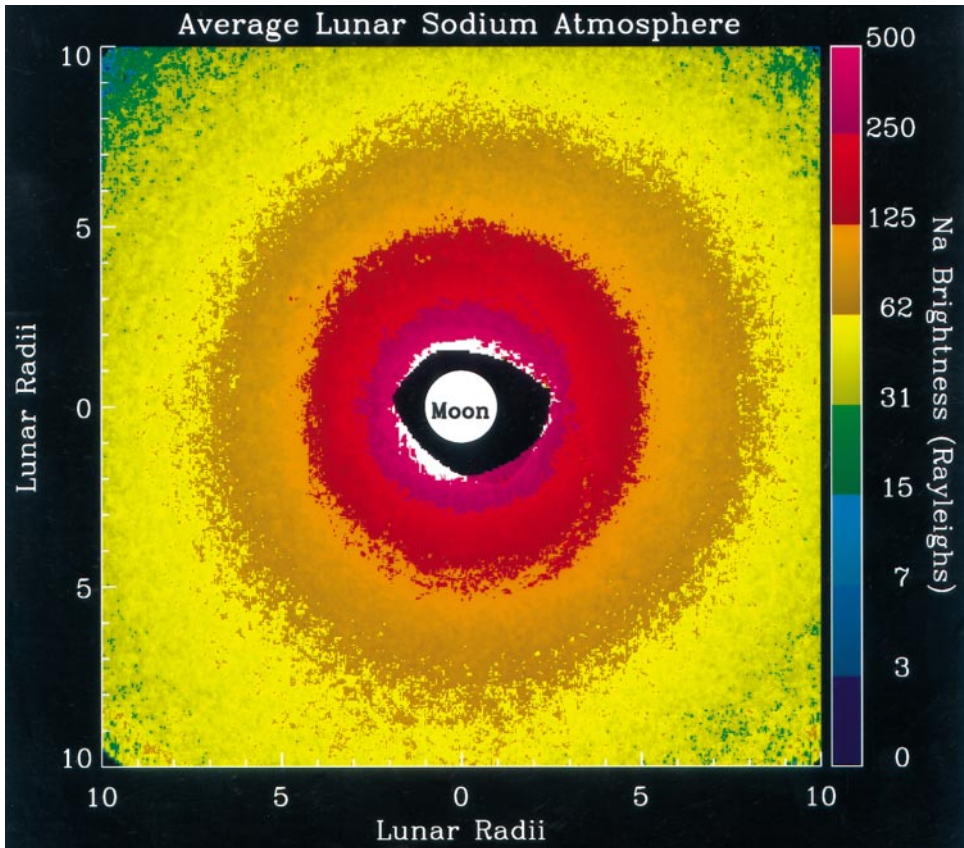


FIG. 7. Average pattern of the Moon’s extended sodium atmosphere at the time of full Moon as observed during four eclipses. The irregular shaped dark area is the sum of the regions close to the Moon not observed during any of the eclipse events shown in Fig. 4. To create an average image, the four events were normalized to the average extrapolated near-surface brightness of 1145 R.

by Cremonese and Verani ($3.5 \pm 2.1 \text{ cm}^{-3}$) to within uncertainties. We expect to derive lower near-surface densities than observers looking closer to the lunar limb since we are only seeing the most extended (hottest) component of the Na atmosphere in our images.

The average vertical profile of number density obeys a power law ($\alpha_n = 2.4$) close to that for a purely escaping atmosphere. If all of the sodium we observe were in escape, then the global Na source rate would be approximately $10^{23} \cdot v \text{ atoms s}^{-1}$, where v is the average vertical velocity of sodium atoms in km/s. Some fraction of the observed atmosphere is probably bound, so this source rate is an upper limit. Previous observationally con-

strained calculations of the source rate vary from 0.1 to 8×10^{23} Na atoms s^{-1} (Potter and Morgan 1988b, Sprague *et al.* 1992, Flynn and Mendillo 1995, Smyth and Marconi 1995).

VI. DISCUSSION AND CONCLUSION

The four eclipse data sets show that the lunar atmosphere remains robust near full Moon, and that it is azimuthally symmetric. The lunar atmosphere extends to more than 12 lunar radii from the Moon, and the $r^{-1.4}$ brightness profile is close to that for a purely escaping atmosphere. This is in marked contrast to the dayside morphology observed at quarter Moon where the brightness pattern of r^{-4} describes a bound coma. Modeling results by Ip (1991), Flynn and Mendillo (1995), and Smyth and Marconi (1995) for quarter Moon conditions have all succeeded in obtaining this pattern using a variety of suprathermal sources, that is, with Na distributions having equivalent temperatures well above those on the surface. Solar radiation pressure creates an extended tail in all such models, and so the notion of an escaping component of the observed atmosphere is not a surprise, especially in consideration of recent arguments for an increased lifetime against photoionization of Na at 1 AU (Huebner *et al.* 1992, Combi *et al.* 1997, Cremonese *et al.* 1997).

TABLE II
Number Density Radial Power Law Parameters

Date	$N_{\text{los}}(\text{limb}) \text{ (cm}^{-2}\text{)}$	$n_0 \text{ (cm}^{-3}\text{)}$	α_n
29/11/93	1.1×10^9	3	2.6
3–4/04/96	1.0×10^9	2	2.2
27/09/96	1.4×10^9	3	2.4
24/03/97	2.2×10^9	5	2.5
Average	1.4×10^9	3	2.4

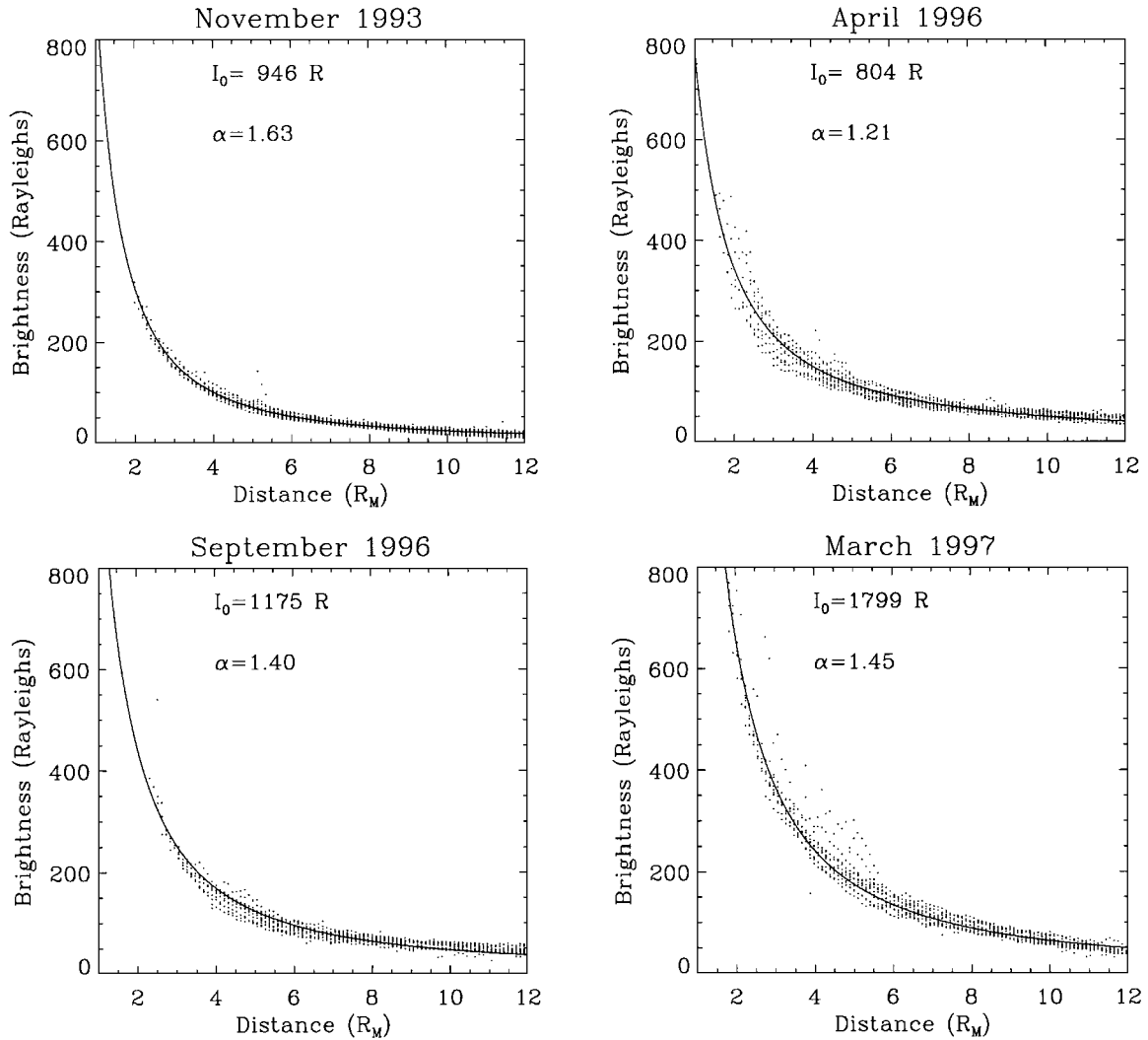


FIG. 5. Radial profiles of the lunar atmosphere with least-squares fit of the power-law $I(r) = I_0 r^{-\alpha}$, where I is the brightness in Rayleighs at distance r (measured in lunar radii, R_M), I_0 is the extrapolated near-surface brightness, and α is the power law index. The data points come from images binned in 30° intervals of position angle and approximately $0.1 R_M$ radial intervals.

In the only model of the lunar atmosphere under full Moon ($\chi = 90^\circ$) conditions, and specifically for the 29 November 1993 eclipse (Mendillo *et al.* 1997b), the power law representation values were $I_0 = 1.8$ kR and $\alpha = 2.3$ for a $\cos^2(\chi)$ -dependent dayside source with a Maxwellian at 1400°K . These are somewhat brighter and represent a more bound atmosphere than the composite image in Figs. 7 and 8 where $I_0 = 1.1$ kR and $\alpha = 1.4$, and the $\chi = 90^\circ$ results at quarter Moon of $I_0 = 1$ kR and $\alpha = 2$ (Flynn and Mendillo 1993). A lunar phase-independent, small-magnitude source of high speed Na, perhaps of micrometeor origin, may well be needed to model these results more accurately. Based on the results of Potter and Morgan (1994), Morgan and Killen (1997) adopted a 60%/40% split in physical (ion) sputtering versus impact vaporization sources to model the lunar atmosphere. Based on the above comparison of our quarter versus full Moon results, we suggest a somewhat larger difference between the impact vaporization source and the solar-zenith-angle-

dependent source. The $\sim 15\%$ spatially independent component of I_0 found by Flynn and Mendillo (1993) may well represent the size needed for future two-component modeling (15% micrometeors and 85% photon-induced desorption). In that context, we note that all four of our eclipse events occurred during periods of minimal meteor activity. The eclipse of 24 March 1997 was the only one during a recognized shower, the Virginids (with a typical peak rate of 5 visible meteors/h at zenith). This is far below more prominent showers, e.g., the Perseids ($\sim 90/\text{h}$) or the Geminids ($\sim 120/\text{h}$). Yet the results in Fig. 4 and Table II do show it to be the brightest of the four events; terrestrial Na was brightest during the April 3–4, 1996 event. We do not consider this data set as an adequate one to judge the importance of meteoritic source effects.

Our preference for photodesorption as the source of the non-thermal Na population that varies with solar zenith angle rests upon a long series of past studies. Measurements using the

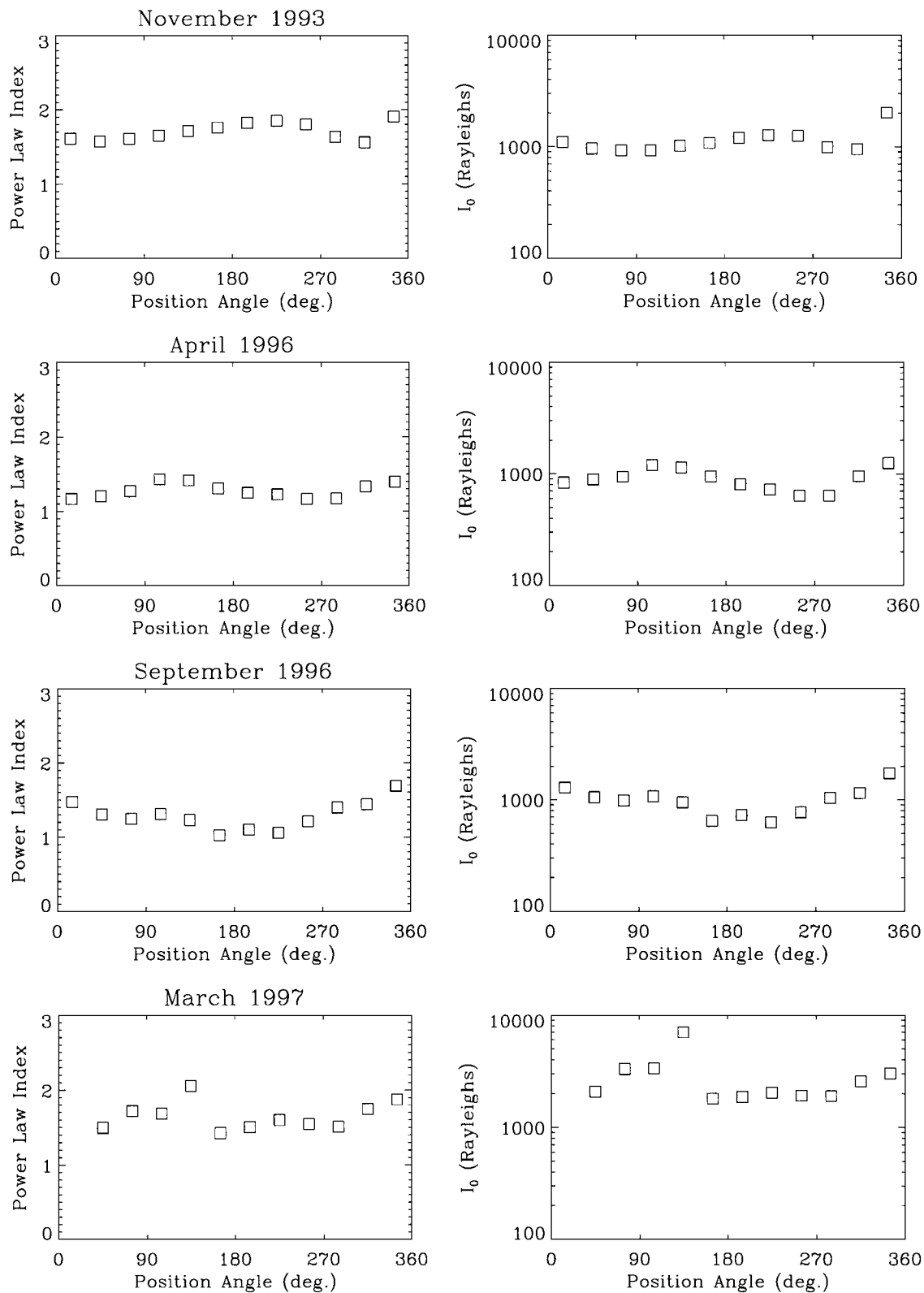


FIG. 6. Radial power law parameters versus position angle, with 0° being north, 90° being west, etc. (Left) Power law index (α), (Right) extrapolated near-surface brightness, for each of the four eclipse datasets.

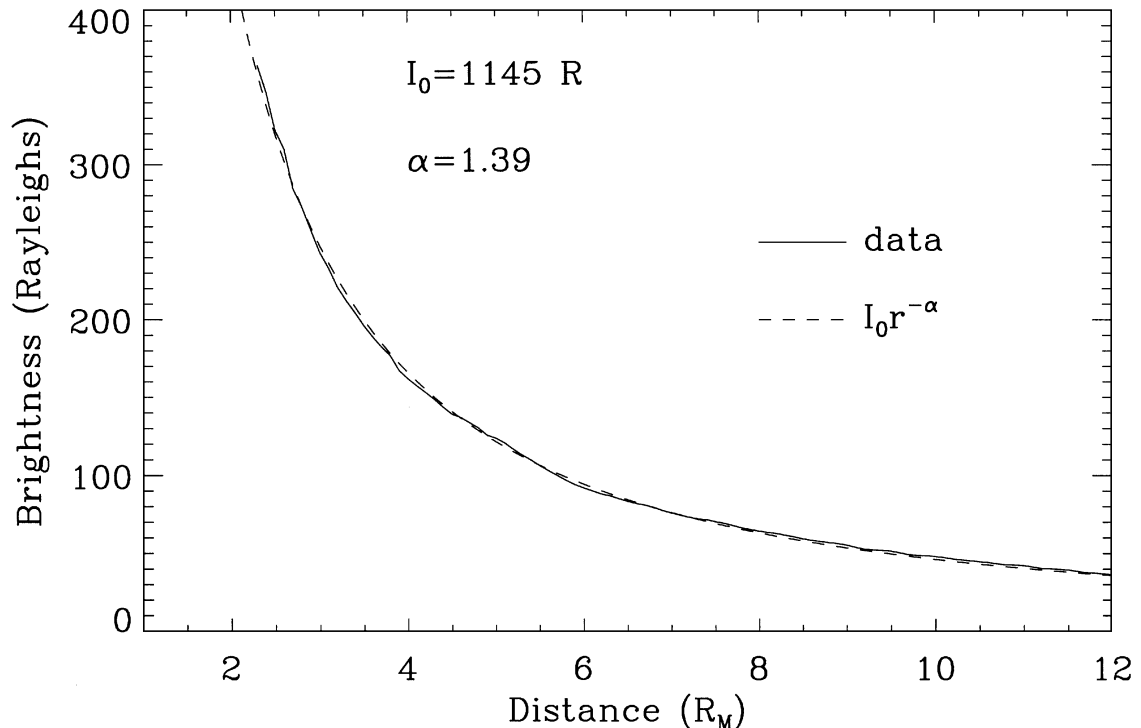


FIG. 8. Average radial profile of sodium ($D_1 + D_2$) brightness at full Moon obtained from four independent observations during lunar eclipse.

Apollo 14 lunar surface package during the total lunar eclipse of 10 February 1971 showed the dramatic effects sunlight has upon the lunar surface (Reasoner and Burke 1972). Hodges *et al.* (1974) made the point that Apollo 16 and 17 data could be modeled successfully using sunlight as the source of energy to release argon from the regolith. After the discovery of sodium and potassium in the lunar atmosphere, Kozłowski *et al.* (1990) and Sprague *et al.* (1992) suggested the same photodesorption mechanism for providing a nonthermal component of the atmosphere. The eclipse results presented here thus offer extraordinary documentation of the extent of space affected by this hot component. The temporary cessation of sunlight during the totality phase is too short to cause a noticeable modification to the sodium atoms seen high above the surface, since their flight times are in hours.

Finally, the existence of an extended lunar atmosphere at full Moon is unquestionably true for the four experiments described here, and yet is enigmatic in the context of the Potter and Morgan (1994) statistical results of low brightness close to the surface of the full Moon. While the full Moon's location in the magnetosphere is an effective isolation site from solar wind impact, the magnetosphere itself is an environment rich in plasma populations. Potter and Morgan (1994) discussed this issue at some length, comparing magnetospheric *in-situ* measurements on the Moon with populations of solar wind ions. They concluded that it is reasonable to expect a substantial reduction in the production of sodium vapor by sputtering when the solar wind is replaced by average magnetospheric lobe or plasma sheet conditions.

For the four periods studied here, solar and geomagnetic activity levels were rather low. As summarized in Table III, the solar radio flux at 10.7 cm (2800 MHz), a parameter long used in solar-terrestrial research as a proxy for solar activity, is close to solar minimum values (October 1996 being the period of absolute solar minimum). The K_p parameter is a 3-h index that characterizes global geomagnetic activity on a log scale from 0 to 9; values of 1 to 4 indicate very quiet to moderate activity (the long-term average value of K_p is 2). Dst is an hourly index (in nT) that portrays classic (equatorial) magnetic field perturbations due to magnetospheric ring currents during a geomagnetic storm. Only the value on 27 September 1996 relates to a period of minor activity. Thus, our preliminary judgment is that no unusual solar or magnetospheric conditions prevailed during these events. Accepting the conclusion of Potter and Morgan (1994) that magnetospheric sources do not replace solar wind sources as equivalent sputtering agents, we conclude that the extended atmospheres portrayed in Fig. 4 are due to neither solar

TABLE III
Geomagnetic Activity

Date	$F_{10.7}$	K_p	Dst (nT)
29/11/93	93.8	2	-11
4/04/96	70.2	3 ⁻	-20
27/09/96	69.8	4	-40
24/03/97	70.1	1 ⁺	2

wind nor magnetospheric ion sputtering sources. The full role of magnetospheric populations impacting the Moon remains to be examined in detail; it will be addressed in a later study. Similarly uncertain is the influence of *chemical sputtering*, in which a chemical reaction occurs between an incident ion (of magnetospheric or solar wind origin) and target atoms, resulting in products desorbed from the surface. Potter (1995) described this possibility with application to Mercury's atmosphere and its potential relevance to the lunar case.

ACKNOWLEDGMENTS

This work was funded in part by NASA Grants NAGS-4991 and NAGW-4917 and by the Center for Space Physics at Boston University. The authors are guest observers at the McDonald Observatory and express their appreciation to the director and staff for continued support of their activities there. We thank C. Barbieri, G. Cremonese, and F. Rampazzi for their assistance in making the April 1996 observations from the TNG facility in La Palma and the director and staff of the Astrophysical Institute of the Canaries for their cooperation and gracious hospitality. We thank A. Morrill and J. Wroten for assistance with observations during the March 1997 eclipse, A. Morrill for subsequent data analysis, and L. Young for helpful discussions.

REFERENCES

- Allen, C. W. 1976. *Astrophysical Quantities*, pp. 169–171. Athlone, London.
- Baumgardner, J., B. Flynn, and M. Mendillo 1993. Monochromatic imaging instrumentation for applications in aeronomy of the Earth and planets. *Opt. Eng.* **32**, 3028–3032.
- Brown, R. A., and Y. L. Young 1993. Io, its atmosphere, and optical emissions. In *Jupiter* (T. Gehrels, Ed.), pp. 1102–1145. Univ. of Arizona Press, Tucson.
- Combi, M. R., M. A. DiSanti, and U. Fink 1997. The spatial distribution on gaseous atomic sodium in the comae of comets: Evidence for direct nucleus and extended plasma sources. *Icarus* **130**, 336–354.
- Cremonese, G., and S. Verani 1997. High resolution observations of the sodium emission from the Moon. *Adv. Space Res.* **19**, 1561–1569.
- Cremonese G., H. Boehnhardt, J. Crovisier, A. Fitzsimmons, M. Fulle, J. Licandro, D. Pollacco, H. Rauer, G. P. Tozzi, and R. M. West 1997. Neutral sodium from Comet Hale–Bopp: A third type of tail. *Astrophys. J.* **490**, L199–202.
- Flynn, B., and M. Mendillo 1993. A picture of the Moon's atmosphere. *Science* **261**, 184–186.
- Flynn, B., and M. Mendillo 1995. Simulations of the lunar sodium atmosphere. *J. Geophys. Res.* **100**, 23,271.
- Hodges, R. R., Jr., J. H. Hoffman, and F. S. Johnson 1974. The lunar atmosphere. *Icarus* **21**, 415–426.
- Huebner, W. F., J. J. Keady, and S. P. Lyon 1992. Solar photo rates for planetary atmospheres and atmospheric pollutants. *Astrophys. Space Sci.* **195**, 1–294.
- Hunten, D. M., R. W. H. Kozlowski, and A. L. Sprague 1991. A possible meteor shower on the Moon. *Geophys. Res. Lett.* **18**, 2101–2104.
- Hunten, D. M., and A. L. Sprague 1997. Origin and character of the lunar and mercurian atmospheres. *Adv. Space Res.* **19**, 1551–1560.
- Ip, W. H. 1991. The atomic sodium exosphere/coma of the Moon. *Geophys. Res. Lett.* **18**, 2093–2096.
- Johnson, R. E. 1990. *Energetic Charged-Particle Interactions with Atmospheres and Surfaces*, pp. 97–121. Springer-Verlag, Berlin.
- Kozlowski, R. W. H., A. L. Sprague, and D. M. Hunten 1990. Observations of potassium in the tenuous lunar atmosphere. *Geophys. Res. Lett.* **17**, 2253–2256.
- Madey, T. E., B. V. Yakshinskiy, V. N. Ageev, and R. E. Johnson 1998. Desorption of alkali atoms and ions from oxide surfaces: Relevance to origins of Na and K in atmospheres of Mercury and the Moon. *J. Geophys. Res.* **103**, 5873–5887.
- Mendillo, M., and J. Baumgardner 1995. Constraints on the origin of the Moon's atmosphere from observations during a lunar eclipse. *Nature* **377**, 404.
- Mendillo, M., J. Baumgardner, G. Cremonese, and C. Barbieri 1997a. Eclipse observations of the lunar atmosphere from the TNG site. In *The Three Galileos: The Man, The Spacecraft, The Telescope* (C. Barbieri, J. Rahe, T. Johnson, and A. M. Sohus, Eds.). Kluwer Academic, Dordrecht.
- Mendillo, M., J. Baumgardner, and B. Flynn 1991. Imaging observations of the extended sodium atmosphere of the Moon. *Geophys. Res. Lett.* **18**, 2097–2100.
- Mendillo, M., J. Emery, and B. Flynn 1997b. Modeling the Moon's extended sodium cloud as a tool for investigating sources of transient atmospheres. *Adv. Space Res.* **19**, 1577.
- Mendillo, M., B. Flynn, and J. Baumgardner 1993. Imaging experiments to detect an extended sodium atmosphere on the Moon. *Adv. Space Res.* **13**, 313–319.
- Morgan, T. H., and R. M. Killen 1997. A non-stoichiometric model of the composition of the atmosphere of Mercury and the Moon. *Planet. Space Sci.* **45**, 81–94.
- Morgan, T. H., and D. E. Shemansky 1991. Limits to the lunar atmosphere. *J. Geophys. Res.* **96**, 1351–1367.
- Potter, A. E. 1995. Chemical sputtering could produce sodium vapor and ice on Mercury. *Geophys. Res. Lett.* **22**, 3289–3292.
- Potter, A. E., and T. H. Morgan 1988a. Discovery of sodium and potassium vapor in the atmosphere of the Moon. *Science* **241**, 675–680.
- Potter, A. E., and T. H. Morgan 1988b. Extended sodium exosphere of the Moon. *Geophys. Res. Lett.* **15**, 1515–1518.
- Potter, A. E., and T. H. Morgan 1991. Observations of the lunar sodium exosphere. *Geophys. Res. Lett.* **18**, 2089–2092.
- Potter, A. E., and T. H. Morgan 1994. Variations of lunar sodium emission intensity with phase angle. *Geophys. Res. Lett.* **21**, 2263–2266.
- Potter, A. E., and T. H. Morgan 1998. Coronagraphic observations of the lunar sodium exosphere near the lunar surface. *J. Geophys. Res. (Planets)* **103**, 8581–8586.
- Reasoner, D. L., and W. J. Burke 1972. Characteristics of the lunar photoelectron layer in the geomagnetic tail. *J. Geophys. Res.* **77**, 6671.
- Roble, R. G., and P. B. Hays 1972. A technique for recovering the vertical number density profile of atmospheric gases from planetary occultation data. *Planet. Space Sci.* **20**, 1727–1744.
- Smyth, W. H., and M. L. Marconi 1995. Theoretical overview and modeling of the sodium and potassium atmospheres of the Moon. *Astrophys. J.* **443**, 371–392.
- Sprague, A. L., D. M. Hunten, R. W. H. Kozlowski, F. A. Grosse, R. E. Hill, and R. L. Morriss 1998. Observations of sodium in the lunar atmosphere during International Lunar Atmosphere Week, 1995. *Icarus* **131**, 372–381.
- Sprague, A. L., R. W. H. Kozlowski, D. M. Hunten, W. K. Wells, and F. A. Grosse 1992. The sodium and potassium atmosphere of the Moon and its interaction with the surface. *Icarus* **96**, 27–42.
- Stern, S. A. 1998. The lunar atmosphere: History, status, current problems, and context. *Rev. Geophys.*, submitted.
- Stern, S. A., and B. C. Flynn 1995. Narrow-field imaging of the lunar sodium atmosphere. *Astron. J.* **109**, 835–841.
- Tyler, A. L., R. W. H. Kozlowski, and D. M. Hunten 1988. Observations of sodium in the tenuous lunar atmosphere. *Geophys. Res. Lett.* **15**, 1141–1144.
- Verani, S., C. Barbieri, C. Benn, and G. Cremonese 1998. Possible detection of Meteor stream effects on the lunar sodium atmosphere. *Planet. Space Sci.* **46**, 1003–1006.